Modeling of spontaneous emission in presence of cylindrical nanoobjects: the scattering matrix approach

V.V. Nikolaev [1], E.I. Girshova [1], M.A. Kaliteevski [2]
[1] Submicron Heterostructures for Microelectronics Research and Engineering Center of the Russian Academy of Science, 194021 St Petersburg, Russia, Politekhnicheskaya, 26;
[2] ITMO University, 197101, St. Petersburg, Russia, Kronverksky Pr., 49

Abstract

We propose a method of analysis of spontaneous emission of a quantum emitter (an atom, a luminescence center, a quantum dot) inside or in vicinity of a cylinder. At the focus of our method are analytical expressions for the scattering matrix of the cylindrical nanoobject. We propose the approach to electromagnetic field quantization based of eigenvalues and eigenvectors of the scattering matrix. The method is applicable for calculation and analysis of spontaneous emission rates and angular dependences of radiation for a set of different systems: semiconductor nanowires with quantum dots, plasmonic nanowires, cylindrical hollows in dielectrics and metals. Relative simplicity of the method allows obtaining analytical and semi-analytical expressions for both cases of radiation into external medium and into guided modes.

Keywords: spontaneous emission, scattering matrix, cylindrical symmetry.
Citation: Nikolaev VV, Girshova EI, Kaliteevski MA. Modeling of spontaneous emission in presence of cylindrical nanoobjects: the scattering matrix approach. Computer Optics 2023; 47(1): 16-26. DOI: 10.18287/2412-6179-CO-1143.

Introduction

Modification and control of spontaneous radiation of quantum emitters is a hot topic of recent decades [1 – 12]. The aim of spontaneous emission manipulation can be achieved with the structures with cylindrical geometry which became technologically accessible and widely researched. Such nanoobjects include semiconductor nanowires [5 – 9, 11 – 17], metallic wires with nanoscale diameters [10], cylindrically perforated metals and dielectrics. Potential applications lay in the arear of single-photon sources [1 – 3, 5, 6], plasmonic metamaterials and nanolasers. Theoretical understanding of spontaneous emission process in such structures is of crucial importance.

Initially the theoretical consideration of spontaneous emission in cylindrical structures was limited to the problem of mode excitation in cylindrical waveguides with approaches based on classical electrodynamics [18, 19]. There were several theoretical methods published which account for radiation from inside a cylinder into external medium [9, 20 – 24, 26 – 28]. Chu and Ho approximated the cylindrical waveguide with a rectangular Fabry–Perot resonator [20]; Nha and Jhe used electrodynamic Green's function technique to calculate radiative-dumping constant of a quantum emitter [21]; Żakowicz and Janowicz used decomposition into cylindrical modes and Fermi's Golden rule with complicated mode quantization approach to resolve a problem of luminescence from dielectric cylinder [22]; Søndergaard and Tromborg [23] used formalism of Green's tensor and quantum-mechanical current operator to study spontaneous emission in active waveguides; Klimov and Ducloy [24] calculated radiation of a classical electric dipole near dielectric nanofiber; Fam Le Kien et al. [25] concentrated attention on emission into the fundamental HE_{11} mode of cylindrical dielectric waveguide. In the paper of A.V. Maslov, M.I. Bakunov, and C.Z. Ning [26] a method based on Fourier integrals [18, 19] is generalized to allow calculation of a dipole radiation intensity from inside a waveguide or a finite-length dielectric cylinder; Henderson et al. [27] made another approach to the problem of classical dipole radiation in vicinity of a waveguide. We recently proposed a relatively simple method for calculation of spontaneous emission from dielectric nanowires which is limited to the case of radial light extraction (with no account for polarization mixing) [28].

Relatively recent advance in this field was made in the paper of Paniagua–Domínguez et al. [9] where external radiation from a dielectric cylinder was treated using so called leaky modes, i.e. continuation of guided modes in the region where these modes acquire imaginary part of propagation wavenumber and become unconfined. The method of Ref. [9] exploits semi-phenomenological approach of a one-dimensional (1D) optical resonator and the induced 1D current to account for the nanowire finate length. In the framework of this approach the researchers examine analogy between Mie resonances and leaky modes [29] and apply their theory to model angular distribution of quantum-dot luminescence from nanowires [30]. In Refs. [31, 32] the emission from nanowire systems with metallic parts are considered.

Despite the wealth of theoretical results on this subject and significant advances made, many researchers use purely numerical methods designed for calculation of a classical dipole radiation in arbitrary dielectric surround-

ings. Such situation might be due to complexity of existing quantum-mechanical methods and leaves limited space to analytical interpretation of numerical and experimental results. The aim of our work is to develop a relatively simple, rigorous and universal theoretical method and present analytical and semi-analytical formulas for spontaneous emission in guided modes and external space for arbitrary position of a quantum emitter in a system containing a cylinder. In the center of our approach is an analytical expression of the optical scattering matrix of a cylinder which could be metallic or dielectric with arbitrary refractive index. We propose a relatively straightforward method of quantization of the modes radiating into external space and solve the problem analytically using eigenvalues and eigenvectors of the scattering matrix of the cylinder. The treatment of the guided modes is consistent with that for radiating modes and is based on the same principles.

1. Optical scattering matrix of homogeneous cylinder

In this work we consider a quantum emitter placed in an arbitrary point inside or outside of an infinitely-long cylinder with the radius ρ_0. The external embedding medium is characterized by the values of dielectric permittivity ε_1 and magnetic permeability μ_1 at the emitter wavelength; and the cylinder is described by parameters ε_2 and μ_2. As a starting point we consider the mode structure of classical electromagnetic fields in a system containing an infinite cylinder. Monochromatic electromagnetic fields can be expressed in a form $\mathrm{Re}\{\boldsymbol{E}(\boldsymbol{r})\exp(-i\omega t)\}$ where the real part is taken from the product of a coordinate-dependent complex- vector field $\boldsymbol{E}(\boldsymbol{r})$ and a time-dependent factor. If a structure possesses cylindrical symmetry in respect to the z axis, one may consider an electric field written in a cylindrical coordinate system (ρ,φ,z) as $\boldsymbol{E}(\boldsymbol{r})=\boldsymbol{E}_m(\rho)\exp(i[k_z z+m\varphi])$ where k_z is the wavenumber of propagation along the symmetry direction, m is an integer number standing for a photon angular momentum. In this work we consider modes which freely propagate along z axis, hence k_z is a real number.

For the subsequent analysis the following dimentionless parameters are important:

$$q=\rho_0 k_0,\quad \tilde{z}=\rho_0 k_z,$$
$$x_1=\sqrt{\varepsilon_1\mu_1 q^2-\tilde{z}^2},\quad x_2=\sqrt{\varepsilon_2\mu_2 q^2-\tilde{z}^2}, \qquad (1)$$

where $k_0=\omega/c$ is the wavevector of emitted light in vacuum, q is the size parameter, $\tilde{z}$ is dimensionless propagation number and $x_{1(2)}$ are external (internal) transverse wavenumbers $k_{\rho i}=\sqrt{\varepsilon_i\mu_i k_0^2-k_z^2}$ multiplied by the radius ρ_0 of the cylinder. Although in this work we consider nonmagnetic materials, we keep magnetic permeabilities in following expressions for the sake of completeness presuming that their values are real and positive. The dielectric permittivities are presumed to be real and can have an arbitrary sign; a negative value of permittivity is reserved for description of a metallic medium below plasmon resonance [10]. Thus, the dimensionless parameters x_1, x_2 can be either real or pure imaginary depending on the wavelength, the values of the propagating constant k_z and the dielectric permitivities. In case the expression $\varepsilon_i\mu_i q^2-\tilde{z}^2$ is negative one should choose the value of the square root from the upper half of complex plain.

The method which we develop in this paper allows to analyze several distinct types of structures and their operating regimes. The type I structure is characterized by the permittivity of the cylinder which is larger than the permittivity of the surrounding medium $\varepsilon_2>\varepsilon_1$, both permitivities are positive. This type of structure corresponds to semiconductor nanowires and nanopillars which can be considered dielectric at the wavelength of a quantum emitter. In this case parameter x_2 is real and positive whereas x_1 is imaginary for guided modes and real for the modes radiating in the external medium.

We designate the opposite case $\varepsilon_2<\varepsilon_1$ as Type II structure; this model structure can be applied to cylindrical hollows ($\varepsilon_2=1$ for air permittivity) etched in a dielectric. In this case x_1 is always real corresponding to the modes radiating into a surrounding dielectric whereas the parameter x_2, which describes the internal field, can be ether real or imaginary.

Our method will also allow to model metallic structures below plasmon resonance where either ε_2 or ε_1 are negative. The negative ε_2 and positive ε_1 (Type III structure) corresponds to metallic nanowires [10] whereas the opposite case (Type IV) can be used to model cylindrical hollows in a metallic film.

If x_1 is real, the field with fixed m and k_z in the external medium can be written as a superposition of converging and diverging propagating waves of TM and TE polarizations:

$$\mathbf{E}_m^{Ext}=\sum_{J=TM,TE}\left(A_J^{+}\tilde{\mathbf{E}}_{J,m}^{Ext+}+A_J^{-}\tilde{\mathbf{E}}_{J,m}^{Ext-}\right), \qquad (2)$$

where $A_{TM/TE}^{+/-}$ are constant amplitude coefficients; the plus (minus) superscript stands for diverging (converging) waves. The axial component of magnetic (electric) field in TM (TE) polarized cylindrical wave is zero; the explicit form of the dimensionless field profiles $\tilde{\mathbf{E}}_{TM/TE,m}^{ext+/-}$ can be found in Appendix A, Eqs. (A1-2).

If parameter x_1 is imaginary the transverse wavenumber $k_{\rho 1}$ is imaginary as well and the fields outside the structure are changing exponentially with the distance from the axis. For the general description of the external fields we can use Eq. (2) with the convention that for imaginary x_1 plus (minus) superscripts stand for the fields exponentially increasing (decreasing) with the growth of the distance ρ from the structure axis; the field profiles for exponentially-changing waves are presented in Appendix A, Eqs. (A4-5). For physically meaningful guided modes exponentially increasing fields are absent.

Due to the requirement of continuity of tangential components of electric and magnetic fields on the cylin-

drical interface the four coefficients $A^{+/-}_{TM/TE}$ are connected to each other. One can write the relation between the plus and minus coefficients of two different polarizations in the matrix form:

$$\begin{pmatrix} A^{+}_{TM} \\ A^{+}_{TE} \end{pmatrix} = \hat{s} \times \begin{pmatrix} A^{-}_{TM} \\ A^{-}_{TE} \end{pmatrix}, \ \hat{s} = \begin{pmatrix} \tilde{r}_{TM\to TM} & \tilde{r}_{TE\to TM} \\ \tilde{r}_{TM\to TE} & \tilde{r}_{TE\to TE} \end{pmatrix}. \tag{3}$$

In this expression quantities $\tilde{r}$ can be considered as analogues of reflection coefficients and the 2×2 matrix $\hat{s}$ composed of these coefficients is a form of the scattering matrix written in a particular basis. Using continuity conditions and the requirement of the finiteness of the fields on the structure axis we derived the explicit expression of the scattering matrix in a general form:

$$\begin{aligned} \tilde{r}_{TM\to TM} &= -\frac{T_{\varepsilon}^{(2)}T_{\mu}^{(1)} - m^2\left(\frac{\tilde{z}}{q}\right)^2 V^2}{R_m(x_1)\Theta}, \\ \tilde{r}_{TE\to TE} &= -\frac{T_{\varepsilon}^{(1)}T_{\mu}^{(2)} - m^2\left(\frac{\tilde{z}}{q}\right)^2 V^2}{R_m(x_1)\Theta}, \\ \tilde{r}_{TE\to TM} &= -i\frac{m\sqrt{\varepsilon_1\mu_1}}{R_m(x_1)\Theta}\frac{\tilde{z}}{q}\frac{V}{Q_m(x_1)}, \\ \tilde{r}_{TM\to TE} &= -\tilde{r}_{TE\to TM}, \end{aligned} \tag{4}$$

with the following designations introduced:

$$\begin{aligned} &\Theta = T_{\varepsilon}^{(1)}T_{\mu}^{(1)} - m^2\left(\frac{\tilde{z}}{q}\right)^2 V^2, \quad V = \frac{1}{x_2^2} - \frac{1}{x_1^2}, \\ &T_{\varepsilon}^{(i)} = \varepsilon_1 F_m^{(i)}(x_1) - \varepsilon_2 G_m(x_2), \\ &T_{\varepsilon}^{(i)} = \mu_1 F_m^{(i)}(x_1) - \mu_2 G_m(x_2). \end{aligned} \tag{5}$$

These expressions contain functions which are defined differently for real and imaginary arguments. For real arguments these functions are:

$$\begin{aligned} &R_m(x) = \frac{H_m^{(1)}(x)}{H_m^{(2)}(x)}, \quad Q_m(x) = i\frac{\pi}{4}x^2 H_m^{(1)}(x)H_m^{(2)}(x), \\ &G_m(x) = \frac{1}{x}\frac{J_m'(x)}{J_m(x)}, \qquad F_m^{(i)}(x) = \frac{1}{x}\frac{H_m'^{(i)}(x)}{H_m^{(i)}(x)}, \end{aligned} \tag{6}$$

where $H_m^{(1/2)}$ are Hankel functions. For a pure imaginary argument $x = i|x|$ these functions are defined as follows:

$$\begin{aligned} &R_m(x) = \frac{I_m(|x|)}{K_m(|x|)}, \qquad Q_m(x) = |x|^2 I_m(|x|)K_m(|x|), \\ &G_m(x) = F_m^{(1)}(x) = -\frac{1}{|x|}\frac{I_m'(|x|)}{I_m(|x|)}, \\ &F_m^{(2)}(x) = -\frac{1}{|x|}\frac{K_m'(|x|)}{K_m(|x|)}, \end{aligned} \tag{7}$$

where I_m and K_m are modified Bessel functions. One can see that for zero photon angular momentum ($m = 0$) or for direction perpendicular to the structure axis ($k_z = 0$, $\tilde{z} = 0$) the scattering matrix is diagonal, which manifests absence of polarization mixing for such conditions [28].

In further analysis we would need to know a relation between the fields outside and inside the cylinder. The field inside the structure can be written as a superposition of field profiles of TM and TE polarizations:

$$\mathbf{E}_m^{Int} = B_{TM}\tilde{\mathbf{E}}_{TM,m}^{Int} + B_{TE}\tilde{\mathbf{E}}_{TE,m}^{Int}. \tag{8}$$

Explicit expressions of field profiles $\tilde{\mathbf{E}}_{TM/TE,m}^{Int}$ can be found in Appendix B, Eqs. (B1,2,5,6). We have found a matrix which connects internal-field coefficients $B_{TM/TE}$ to the external coefficients $A^{-}_{TM/TE}$ of converging or exponentially decreasing waves:

$$\begin{aligned} &\begin{pmatrix} B_{TM} \\ B_{TE} \end{pmatrix} = \hat{\tilde{B}}^{Int} \times \begin{pmatrix} A^{-}_{TM} \\ A^{-}_{TE} \end{pmatrix}, \\ &\hat{\tilde{B}}^{Int} = -\frac{1}{2}\sqrt{\frac{\mu_2}{\mu_1}}\frac{1}{\Theta}\frac{1}{Q_m(x_1)}\frac{x_1}{x_2}\frac{Z_m^{(2)}(x_1)}{Z_m^{(1)}(x_2)} \times \\ &\times \begin{pmatrix} \sqrt{\varepsilon_1\varepsilon_2}T_{\mu}^{(1)} & im\sqrt{\varepsilon_2\mu_1}\frac{\tilde{z}}{q}V \\ -im\sqrt{\varepsilon_1\mu_2}\frac{\tilde{z}}{q}V & \sqrt{\mu_1\mu_2}T_{\varepsilon}^{(1)} \end{pmatrix}. \end{aligned} \tag{9}$$

Here we introduced designations for the functions $Z_m^{(1/2)}(x)$. For real arguments they coincide with the following Bessel functions:

$$Z_m^{(1)}(x) = J_m(x), \quad Z_m^{(2)}(x) = H_m^{(2)}(x), \tag{10}$$

and for imaginary x these designations stand for the modified Bessel functions:

$$Z_m^{(1)}(x) = I_m(|x|), \qquad Z_m^{(2)}(x) = K_m(|x|). \tag{11}$$

Similarly to the scattering matrix, the matrix $\hat{\tilde{B}}^{Int}$ is diagonal for $m = 0$ or $k_z = 0$, $\tilde{z} = 0$.

2. Spontaneous emission of a quantum emitter

Let us consider a quantum emitter placed at the point $\mathbf{r}_0$ with an optical transition characterized by the dipole matrix element $\mathbf{d}_{fi} = |\mathbf{d}_{fi}|\mathbf{e}_d$ ($\mathbf{e}_d$ is a complex vector of optical-transition polarization). Spontaneous emission rate can be calculated using Fermi's Golden Rule:

$$W = \frac{\pi}{2\hbar}\left|\mathbf{d}_{fi}\right|\sum_p \left|\mathbf{E}_p(\mathbf{r}_0)\cdot\mathbf{e}_d\right|^2 \delta(\hbar\omega_{fi} - \hbar\omega_p), \tag{12}$$

where $\hbar\omega_{fi}$ is the energy of the optical transition and $\mathbf{E}_p(\mathbf{r}_0)$ is the complex amplitude of the electric field of a quantized mode at the location of the emitter. The subscript p stands for the mode quantization numbers; the real electric field of the mode is calculated as $\mathrm{Re}\{\mathrm{Epexp}(-i\omega_p t)\}$. The optical mode should be quantized and nor-

malized so that the total electromagnetic energy inside a quantization volume is equal to the single photon energy $\hbar\omega_p$. Summation in Eq. (12) is taken over all possible quantized optical modes.

It is natural for the considered problem to take quantization figure in a form of a cylinder which z axis coincides with the symmetry axis of the structure; the radius R and the height L_z of the quantization cylinder are put to infinity at the final stage.

On the top and bottom facets of a quantization cylinder the standard Born–von Karman periodic boundary condition can be used [20] which discretizes the propagation wavenumber k_z or the parameter $\tilde{z}$. The differential of the mode number connected with the light propagation along the axis is

$$dN_z = \frac{L_z}{2\pi} dk_z. \tag{13}$$

In the expression (12) one can substitute summation over the discrete quantum number N_z with integration over the propagation wavenumber differential dk_z.

2.1. Radiation into external medium

Emission of a quantum emitter into external medium can be analyzed as follows. If the conditions are such that the parameter x_1 and the transverse wavenumber $k_{\rho 1}$ are real (see Eq. (1)), the field outside the cylinder is a superposition of converging and divergent cylindrical waves of TM and TE polarizations, Eq. (2). For spontaneous-emission calculation a quantization procedure for such modes should be devised.

We propose a simple and straightforward quantization condition: the electric field components tangential to the cylindrical surface of the quantization cylinder should be equated to zero. Such procedure has a distant analogy to quantization of electron-hole pairs in quasi-continuous part of spectrum (the Elliott formula).

Let us introduce an auxiliary matrix:

$$\begin{gathered}\hat{M} = \exp\left(i\left[2x_1 \frac{R}{\rho_0} - m\pi - \frac{\pi}{2} \right] \right) \times \hat{\tilde{s}}, \\ \hat{\tilde{s}} = \begin{pmatrix} \tilde{r}_{TM\to TM} & \tilde{r}_{TE\to TM} \\ -\tilde{r}_{TM\to TE} & -\tilde{r}_{TE\to TE} \end{pmatrix},\end{gathered} \tag{14}$$

where $\hat{\tilde{s}}$ can be obtained from the cylinder scattering matrix $\hat{s}$ Eqs. (3, 4) by multiplication of the lower row by –1. Using the relation between coefficients of convergent and divergent waves Eq. (3) and asymptotics of Hankel functions at large arguments one can show that the requirement of zero transverse electric field components at the quantization cylindrical surface in the limit $R\to\infty$ is equivalent to equality of the matrix $\hat{M}$ eigenvalue to minus one:

$$\exp\left(i\left[2x_1 \frac{R}{\rho_0} - m\pi - \frac{\pi}{2} \right] \right) \times \tilde{\beta}^{\pm} = -1, \tag{15}$$

where $\tilde{\beta}^{\pm}$ are the eigenvalues of the matrix $\hat{\tilde{s}}$:

$$\begin{gathered}\tilde{\beta}^{\pm} = \frac{\tilde{r}_{TM\to TM} - \tilde{r}_{TE\to TE}}{2} \pm \frac{\tilde{r}_{TM\to TM} + \tilde{r}_{TE\to TE}}{2} \times D, \\ D = \sqrt{1 - 4\frac{\tilde{r}_{TE\to TM}\tilde{r}_{TM\to TE}}{\left(\tilde{r}_{TM\to TM} + \tilde{r}_{TE\to TE}\right)^2}}.\end{gathered} \tag{16}$$

In addition, for the quantized mode the pair of coefficients $\{A^-_{TM}, A^-_{TE}\}$ is an eigenvector of matrix $\hat{M}$ and consequently is an eigenvector of the modified scattering matrix of the cylinder $\hat{\tilde{s}}$. This conclusion allows to obtain relations between polarizations in the quantized radiating modes:

$$A^-_{TE} = -\frac{\tilde{r}_{TM\to TE}}{\tilde{r}_{TE\to TE} + \tilde{\beta}^{\pm}} A^-_{TM}, \tag{17a}$$

$$A^-_{TM} = -\frac{\tilde{r}_{TE\to TM}}{\tilde{r}_{TM\to TM} - \tilde{\beta}^{\pm}} A^-_{TE}. \tag{17b}$$

Coefficients for the divergent waves can be expressed through the coefficients of the convergent waves using the scattering matrix Eq. (3). Thus we show that the proposed quantization procedure produces analytical expressions for the polarization mode structure which depends on the cylinder reflection properties (the analytical expressions of $\tilde{r}$ coefficients for different types of cylinders were presented in the previous chapter, see Eq. (4, 8)).

Let us analyze the obtained results. If the conditions are such that mixing of TM and TE polarizations are weak or absent (when $m=0$ or the radiation propagates perpendicularly to the axis, i.e. $k_z\approx 0$, $\tilde{z}\approx 0$, $\theta\approx\pi/2$) then cross-coefficients go to zero $\tilde{r}_{TM\to TE}\to 0$, $\tilde{r}_{TE\to TM}\to 0$ and one obtains

$$\begin{gathered}D\to 1, \\ \tilde{\beta}^{+}\to \tilde{r}_{TM\to TM}, \\ \tilde{\beta}^{-}\to -\tilde{r}_{TE\to TE}.\end{gathered} \tag{18}$$

Thus at weak mixing conditions the quantized mode corresponding to the eigenvalue $\tilde{\beta}^{+}$ transforms into a pure TM mode, whereas $\tilde{\beta}^{-}$ modes approach TE modes. Such transformation is typical for a cylindrical waveguide mode: EH-modes approach pure TM modes and HE-modes go to TE modes with the decrease of the waveguide dielectric contrast. Therefore we can label radiating modes at perpendicular propagation angle corresponding to $\tilde{\beta}^{+}$ as EH (or TM-like) modes, and the quantized modes corresponding to $\tilde{\beta}^{-}$can be considered as HE (or TE-like) modes. At an arbitrary propagation angle we choose the sign in Eq. (18) in such manner that the angular dependencies of $\tilde{\beta}^{+}(\theta)$ are everywhere continuous. Considering Eq. (17) one can see that the expression (17*a*) can be more conveniently used for EH modes and expression (17*b*) suits HE modes since in this case correct polarizations are obtained in the vicinity of the perpendicular propagation angle. Therefore we can state that another quantum number designating external radiative modes labels polarization and can be either EH or

HE corresponding to the different eigenvalues $\tilde{\beta}^{+}$ of the modified scattering matrix.

To be able to use these modes for spontaneous-emission calculation Eq. (12) one needs to normalize them:

$$\int_{V_c} u_p(\mathbf{r})\, dV = \hbar\omega_p, \tag{19a}$$

$$u_p(\mathbf{r}) = \frac{1}{16\pi}\left(\varepsilon(\mathbf{r})\left|\mathbf{E}_p(\mathbf{r})\right|^2 + \mu(\mathbf{r})\left|\mathbf{H}_p(\mathbf{r})\right|^2\right), \tag{19b}$$

where integration of electromagnetic energy density $u_p(\mathbf{r})$ over the volume V_c of the quantization cylinder is performed (in this work the Gaussian unit system is used). In case of modes radiating into external space this integral goes to infinity with the increase of the size of quantization cylinder. Therefore, for normalization procedure we can consider the asymptotic form of cylindrical waves at large distances which transform into local plain waves (see Appendix A, Eq. (A3)). Hence we obtain the normalization condition

$$\left|A_{TM}^{-}\right|^2 + \left|A_{TE}^{-}\right|^2 = \frac{4\pi}{L_z R}\frac{x_1}{\rho_0\varepsilon_1}\hbar\omega_p. \tag{20}$$

In (20) it is presumed that any light absorption or generation in the cylindrical structure can be neglected.

The quantization condition Eq. (15) can be analyzed as follows. In the absence of absorption or generation the absolute values of the modified scattering matrix eigenvalues are always equal to unity $|\tilde{\beta}^{\pm}|=1$, which is the consequence of the energy-flux conservation. Thus Eq. (15) imposes restriction on the phase of the complex number on the right hand side. When the quantization-cylinder diameter R is large the main contribution into phase variation stems from the exponential factor whereas variation of the phase of the eigenvalue $\tilde{\beta}^{\pm}$ can be neglected. This gives us a quasi-discrete spectrum of the radiating modes, and the differential of the mode quantum number related to the transverse field distribution is:

$$dN_\rho = \frac{R}{\pi}\frac{dx_1}{\rho_0}. \tag{21}$$

As a result, the summation over photon modes in Fermi's Golden Rule can be expressed as

$$\begin{aligned}&\sum_p \rightarrow \sum_m \sum_{J=\mathrm{EH,HE}} \sum_{N_z}\sum_{N_\rho} \rightarrow \\ &\rightarrow \sum_m \sum_{J=EH,HE} \frac{L_z}{2\pi}\int dk_z \frac{R}{\pi}\int \frac{dx_1}{\rho_0}.\end{aligned} \tag{22}$$

A number of radiating modes with fixed m and polarization $J=\mathrm{EH}/\mathrm{HE}$ in an interval of photon energies $[\hbar\omega_p, \hbar\omega_p + d(\hbar\omega_p)]$ can be written as:

$$dN_{m,J} = dN_\rho dN_z = \varepsilon_1\mu_1 \frac{RL_z}{2\pi^2}\frac{\hbar\omega_p}{(\hbar c)^2} d\theta d(\hbar\omega_p), \tag{23}$$

where θ is the angle between the symmetry axis and the propagation direction of cylindrical waves at large distances ($\tan\theta = x_1/\tilde{z} =$, see Appendix A, Eq. (A3)). To obtain the analogue of the photonic density of states Eq. (25) from Eq. (24) we used the dispersion relation between the light wavevector and frequency in the external medium $k_1 = \sqrt{k_{\rho 1}^2 + k_z^2} = \sqrt{\varepsilon_1\mu_1}\,\omega/c$ with the help of which an area element in the $\{k_{\rho 1}, k_z\}$ half-plane can be transformed

$$\begin{aligned}&dk_z \frac{dx_1}{\rho_0} = dk_z dk_{\rho 1} \rightarrow \\ &\rightarrow k_1 d\theta dk_1 = \varepsilon_1\mu_1 \frac{\omega}{c^2} d\theta d\omega.\end{aligned} \tag{24}$$

Rewriting Eq. (12) using Eqs. (20, 22, 23) we obtain the expression for the spontaneous emission rate W_{rad} into external radiating modes:

$$\begin{aligned}&W_{rad} = \frac{3}{4} W_1 \times \\ &\times \sum_{m=-\infty}^{+\infty} \sum_{J=EH,HE} \int_0^{\pi} \frac{\left|\tilde{\mathbf{E}}_{J,m}^{*}(\rho_0)\cdot\mathbf{e}_d\right|^2}{1+C_m} \sin\theta d\theta, \\ &W_1 = \frac{4}{3}\mu_1\sqrt{\varepsilon_1\mu_1}\,\frac{\omega_{fi}^3}{\hbar c^3}\left|\mathbf{d}_{fi}\right|^2,\end{aligned} \tag{25}$$

where the coefficients C_m were introduced (see Eq. (17))

$$\begin{aligned}&C_m = \left|\frac{A_{TE}^{-}}{A_{TM}^{-}}\right|^2_{\tilde{\beta}=\tilde{\beta}^{+}} = \left|\frac{A_{TM}^{-}}{A_{TE}^{-}}\right|^2_{\tilde{\beta}=\tilde{\beta}^{-}} = \\ &= \frac{\left|\tilde{r}_{TM\to TE}\right|^2}{\left|\tilde{r}_{TE\to TE} + \tilde{\beta}^{+}\right|^2} = \frac{\left|\tilde{r}_{TE\to TM}\right|^2}{\left|\tilde{r}_{TM\to TM} - \tilde{\beta}^{-}\right|^2},\end{aligned} \tag{26}$$

which stem from the mode normalization Eq. (19). One can see that $C_m = 0$ when the polarization mixing is absent.

In Eq. (25) the quantity $\tilde{\mathbf{E}}_{J=\mathrm{EH/HE},m}^{*}$ is a dimensionless electric-field profile of the quantized radiating mode of the structure. This complex vector field is formed as follows. For EH (HE) polarization one should put $A_{TM}^{-}=1$ ($A_{TE}^{-}=1$) and the equation (17a) (equation (17b)) should be used for calculating another converging-wave coefficient. The coefficients of the outgoing cylindrical waves (A_{TM}^{+}, A_{TE}^{+}) and of the field inside the cylindrical structure (B_{TM}, B_{TE}) are obtained using the matrix expressions Eq. (4) and Eq. (10) respectively. Since the elements of the matrices $\hat{s}$ and $\hat{B}^{Int}$ were obtained analytically, one can find an analytic expressing for $\tilde{\mathbf{E}}_{J,m}^{*}$ in any point inside and outside the cylindrical structure and use it in Eq. (25) to calculate spontaneous emission of a quantum emitter placed at that point.

One can see that parameters of quantization cylinder R and L_z do not enter the final expression Eq. (25). If the quantum emitter is placed on the cylinder axis, one should restrict angular momentum numbers to $m=-1, 0, 1$ because the modes with $|m|>1$ have zero electric field at the axis (see Appendix B).

2.2. Spontaneous emission into guided modes

Let us consider the case when the parameter x_1 is imaginary (or the transverse wavenumber $k_{\rho 1}$ is imaginary, see Eq. (1)). This situation may occur for the nanowire (type I structure) in a waveguide regime or for the cylindrical hollow in a metal film (type IV structure). In this case the plus coefficients $A^{+}_{TM/TE}$ in Eq. (2) at exponentially increasing fields should be equal to zero. In the matrix form, Eq. (3), this condition is written as

$$\begin{pmatrix} 0 \\ 0 \end{pmatrix} = \hat{s} \times \begin{pmatrix} A^{-}_{TM} \\ A^{-}_{TE} \end{pmatrix}, \tag{27}$$

and similarly for the modified scattering matrix $\hat{\tilde{s}}$. This leads to the requirement of degeneracy of the scattering matrices:

$$\begin{aligned} &\det\left[\hat{s}\left(q,\tilde{z}\right)\right] = \det\left[\hat{\tilde{s}}\left(q,\tilde{z}\right)\right] = 0, \\ &\tilde{r}_{TE\to TE}\tilde{r}_{TM\to TM} = \tilde{r}_{TM\to TE}\tilde{r}_{TE\to TM}. \end{aligned} \tag{28}$$

For the type I structure this condition reduces to the standard dispersion equation of the cylindrical waveguide. The equation (28) produces the dispersion dependence between the mode frequency and the propagation wavenumber for a particular guided mode ν with an angular number m:

$$\begin{aligned} &q = q_{m,\nu}\left(\tilde{z}\right), \\ &\omega = \omega_{m,\nu}\left(k_z\right). \end{aligned} \tag{29}$$

From such dispersion relations group velocities of guided modes can be found

$$v^{g}_{m,\nu} = \frac{d\omega_{m,\nu}\left(k_z\right)}{dk_z}. \tag{30}$$

The relations between external exponentially-decreasing fields of different polarizations are defined by Eq. (27):

$$\begin{aligned} A^{-}_{TE} &= -\frac{\tilde{r}_{TM\to TE}}{\tilde{r}_{TE\to TE}} A^{-}_{TM}, \\ A^{-}_{TM} &= -\frac{\tilde{r}_{TE\to TM}}{\tilde{r}_{TM\to TM}} A^{-}_{TE}. \end{aligned} \tag{31}$$

The fields inside the cylinder can be found from Eq. (10).

The summation over guided modes in Eq. (12) takes the form:

$$\begin{aligned} &\sum_{p} \to \sum_{m}\sum_{\nu}\sum_{N_z} \to \\ &\sum_{m}\sum_{\nu}\frac{L_z}{2\pi}\int dk_z \to \frac{L_z}{2\pi}\sum_{m}\sum_{\nu} 2\int\limits_{\omega^{c}_{m,\nu}}^{+\infty} \frac{1}{\hbar v^{g}_{m,\nu}} d\left(\hbar\omega\right), \end{aligned} \tag{32}$$

where Eqs. (13) and (30) were used; $\omega^{c}_{m,\nu}$ is the cut-off frequency of the guided mode. Normalization of the electromagnetic energy of a guided mode in a cylinder of height L_z leads to the following expression for the spontaneous emission rate into a particular guided mode with quantum numbers m and ν:

$$\begin{aligned} W^{m,\nu}_{WG} &= \frac{1}{2}\frac{\omega_{fi}}{\hbar v^{g}_{m,\nu}}\left|\mathbf{d}_{fi}\right|^2 \frac{1}{S_{m,\nu}} \times \\ &\times\left|\mathbf{E}^{m,\nu}_{WG}\left(\rho_0,\omega_{fi}\right)\cdot\mathbf{e}_d\right|^2 H\left(\omega_{fi}-\omega^{c}_{m,\nu}\right), \end{aligned} \tag{33}$$

where $H(\omega)$ is the Heaviside function, $\mathbf{E}^{m,\nu}_{WG}$ is the mode electric field and

$$S_{m,\nu} = 2\pi\int\limits_{0}^{+\infty} u_{m,\nu}\left(\rho\right)\rho d\rho \tag{34}$$

is the normalization integral of the mode energy density Eq. (19b) over the plain perpendicular to the symmetry axis. In Eq. (34) the field profile $\mathbf{E}^{m,\nu}_{WG}$ can be scaled arbitrary provided that that the same field is used in calculation of the energy density Eq. (19b), Eq. (34). For calculation of field profiles in an arbitrary point of the structure one can employ Eq. (2) for external fields and Eq. (9) for internal fields putting $A^{+}_{TM/TE} = 0$; the relation between coefficients $A^{-}_{TM/TE}$ is fixed by Eq. (31) and the internal-field coefficients $B_{TM/TE}$ are given by the general matrix relation Eq. (10).

3. Results and discussion

We apply obtained theoretical results to calculate Purcell factors for quantum emitters placed in GaN nanowires. The Purcell factor is defined as a ratio of the spontaneous emission rate of an emitter into a particular channel to the emission rate of that emitter placed into homogeneous bulk GaN. The refractive index of GaN is taken to be equal to 2.4 which approximately corresponds to the yellow-green region of the spectrum [33]. The emitter emission wavelength is taken to be 550 nm to simulate radiation of InGaN quantum dots [34]. The radiating quantum dot is placed at the center of the nanowire; the length of the nanowire is considered to be large enough to apply an infinite waveguide approximation.

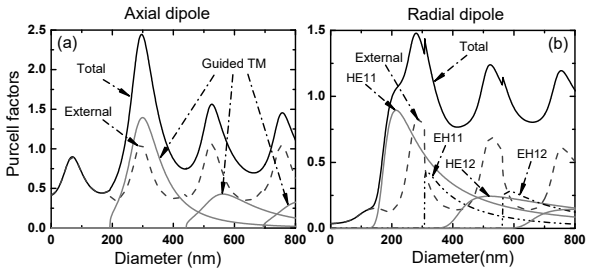

Fig. 1. Purcell factors of an InGaN quantum dot (emission wavelength 550 nm) placed in the center of a GaN nanowire as functions of nanowire diameter. In the left panel (a) the optical-transition matrix element is directed along the nanowire axis (axial orientation); in panel (b) the matrix element is perpendicular to the axis (radial orientation)

In Fig. 1 calculation of the Purcell factors for a InGaN quantum dot in a GaN nanowire (NW) is shown. In the

left panel the radiating optical transition is described by a linear dipole directed along the NW axis; in the right panel the direction of the dipole is perpendicular to the axis. The latter case can be considered as corresponding to the circularly-polarized transition or as a radiation of a linear dipole averaged by its direction perpendicular to the axis. One may see that both external and guided channels of radiation significantly influence the total spontaneous emission.

Maxima in the external emission seen in Fig. 1 occur due to microcavity effect [35] or the Purcell enhancement induced by the light confinement in the lateral directions. One may see in Fig. 1 that distance between diameters at which maxima appear approximately coincide with the emission wavelength in the material of the cylinder (230 nm in the considered example). In the simple case when an emitter is placed in the center of a one-dimensional (1D) Fabry-Perot cavity resonant conditions are satisfied when the length of the resonator is exactly equal to the odd number of half-wavelengths in the cavity material. The considered case of cylindrical geometry and the emitter which can radiate light at any angle is more complicated than the 1D case. This can be seen in Fig. 1 where Purcell enhancement peaks are broad and the positions of their maxima do not follow the simple Fabry-Perot rule, but the tendency to have wavelength distance between maxima is recovered at larger diameters.

As the diameter of the nanowire increases new guided modes appear and start to participate in the radiation process. When the diameter exceeds the cut-off value the emission in that particular mode quickly reaches maximum but with further diameter increase the electric field of the guided mode at the cylinder axis decreases. Thus the decrease of the guided-mode confinement factor at the emitter position stipulates the decline of the mode interaction with the emitter.

In Fig. 1 one may see that emergence of new guided modes (TM-polarized for axial-dipole case and EH-polarized for radial case) coincide with the decrease of the luminescence in radiative modes. In the axial-transition case the diameter at which radiation in external space is maximal approximately coincides with that for guided-mode luminescence.

Thus an important finding evident in our calculation results (Fig. 1) is a direct correlation between emission into external space and the waveguide emission. We would like to stress attention that our formalism of spontaneous emission into radiative modes summarized in the expression (25) does not contain any artificial provision for guided modes and their cut-off frequencies. Therefore, the attained correlation between external and waveguide radiation is naturally embedded in our formalism and shows that the two parts of the developed theory are self-consistent.

From Fig. 1*b* one may see that dependencies of the HE Purcell factors on diameter are qualitatively different from that for EH modes. Indeed, the radiation into HE-polarized modes commences evenly starting from zero values at cut-off diameters whereas luminescence into EH modes shows threshold-like character at cut-off conditions with an abrupt jump of the Purcell factor. This effect is due to different behavior of the group velocities of HE and EH modes at cut-off.

Our results for GaN nanowires presented in Fig. 1*b* are qualitatively similar to purely-numerical calculations obtained by the J.M. Gerard scientific group for GaAs nanowires of finite length and radial dipole orientation, see Refs. [3, 6 – 8]. In the paper of Claudon et al. Ref. [6] in Fig. 1 numerical calculations of external and guided mode Purcell factors are shown and one can see sharp drop in the external emission at the cut-off diameter of a new guided mode. This behavior closely matches our semi-analytical calculations in Fig. 1*b*, although the authors of Ref. [6] attribute the guided mode as HE_{12} whereas we conclude that it is EH_{11} mode.

In the limiting case of small diameters, the spontaneous emission is suppressed by dielectric screening of a dipole inside a nanowire [6-8, 18, 26]. In thin nanowires the analytical expressions for Purcell factors of axial (P_{ax}) and radial (P_{rad}) dipoles are known [26]:

$$P_{ax} = \sqrt{\frac{\varepsilon_1}{\varepsilon_2}}, \qquad P_{rad} = \sqrt{\frac{\varepsilon_1}{\varepsilon_2}}\left(\frac{2\varepsilon_1}{\varepsilon_1+\varepsilon_2}\right)^2. \tag{35}$$

For a GaN nanowire (the refractive-index value is 2.4) in air these Purcell factors are $P_{ax}=0.417$, $P_{rad}=0.0365$ and strong suppression of the radial-transition radiation is evident.

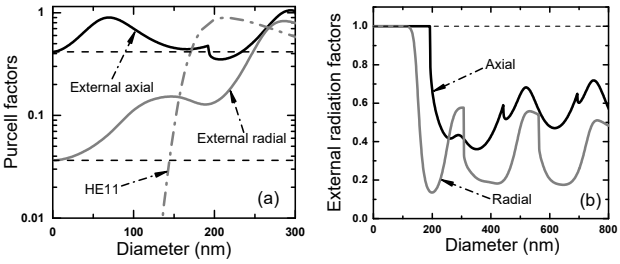

Fig. 2. (a) External-radiation Purcell factors from a GaN nanowire for smaller diameters shown in logarithmic scale; dashed horizontal lines correspond to Eq. (35) . The Purcell factor for a radial dipole radiation into the fundamental HE_{11} mode is also shown. (b) External radiation factors as functions of the nanowire diameter for axial and radial optical-transition orientation

In Fig. 2*a* the Purcell factors in smaller-diameter region are shown in logarithmic scale. One can see that our calculations exactly match the analytical values Eq. (35) when the diameter goes to zero (dashed lines in Fig. 2*a*). It can be seen in Fig. 2*a* that despite the existence of the fundamental HE_{11} mode in the small-diameter region the emission in that mode is negligible due to the weak light localization inside NW. The onset of spontaneous emission into the fundamental HE_{11} mode happens when the nanowire diameter exceeds the value of approximately 130 nm.

In Fig. 2*b* external radiation factors are shown which are defined as ratios of a luminescence intensity in exter-

nal space to the total luminescence intensity including radiation in guided modes. One can see that the fraction of radiation that goes directly into surrounding space is always significant for axial optical transitions. This suggests that one cannot limit consideration of the spontaneous emission process to guided modes in such material system. At small diameters there are no guided modes interacting with the axial transition, thus all luminescence is transmitted by external radiating modes. At the same time the radial transition directs almost all its luminescence in external space despite the formal existence of the fundamental HE_{11} mode at small diameters (see Fig. 2*a*). It is evident that in the radial case the variation of the external radiation factor is strong and diameter regions exist where relative external luminescence is either suppressed or enhanced; but the external radiation factor newer falls to zero value showing that it is not possible to direct total spontaneous emission in guided modes in the considered system.

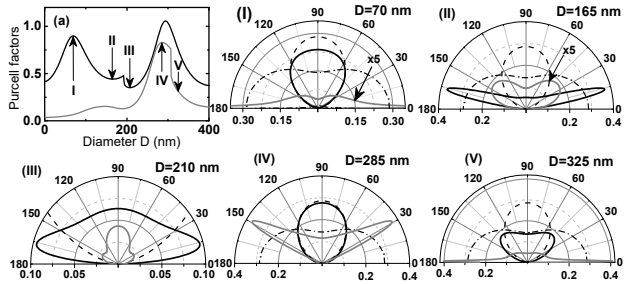

Fig. 3. Angular dependence of spontaneous emission from GaN nanowires of different diameters D: 70 nm (I), 165 nm (II), 210 nm (III), 285 nm (IV) and 325 nm (V). Black (gray) curves show normalized spontaneous emission rate inside a solid angle for axial (radial) dipole direction; dashed (dash-dotted) curves depict angular distribution of emission for an axial (averaged radial) dipole transition in bulk GaN. The panel (a) shows external-emission Purcell factors; arrows point the NW diameters under investigation

In Fig. 3 we examine angular dependence of spontaneous emission of a quantum emitter placed in the center of a nanowire; the emission rates in particular solid angles are normalized to the total emission rate of a dipole in air. It is evident that directionality of emission strongly depends on the nanowire diameter for both axial and radial dipole-transition orientations. One may list the following findings: a) at NW diameters when the total external emission of the axial dipole reaches local maxima (panels (I) and (IV) in Fig. 3) the radiation of that type of optical transition has preferable direction perpendicular to the NW axis resembling the case of a dipole emission in homogeneous medium; b) when the NW diameter approaches the cut-off condition from below (panel (II) for TM mode interacting with the axial dipole and panel (IV) for EH_{11} mode interacting with the radial dipole) the spontaneous radiation of the corresponding optical transition becomes highly directional and the light tends to propagate at sharp angles to the NW axis; c) when the diameter passes the cut-off (panels III and V) the angular distributions of emission intensity change abruptly switching from a highly directional regime to more homogeneous one.

Conclusions

We have developed a theoretical approach which allows calculation and analysis of spontaneous radiation of a quantum emitter in a presence of a cylinder. The position of the emitter can be arbitrary (inside or outside the cylinder) and the refractive index of the cylinder can exceed or be less than the refractive index of the surrounding medium. The dielectric permittivity of the cylinder or the medium in which it is placed can be negative as in the case of metals below plasmonic resonance. Therefore, our method allows modeling of spontaneous emission in a variety of structures such as semiconductor nanowires, cylindrical hollows in dielectric substrates, plasmon waveguides and metals with cylindrical perforation. Our method accounts for emission into external space as well as for radiation channeling into guided modes.

We applied our method to investigation of spontaneous emission from GaN nanowires. We had researched dependence of Purcell factors on the nanowire diameter; comparison of the emission intensities into external medium and into different guided modes was performed. We have found strong correlation between radiation in external space and into guided modes. In particular, we have shown that when the values of parameters of the structure cross cut-off conditions for guided modes qualitative and abrupt quantitative changes in spontaneous emission occur. It is shown that directionality of spontaneous emission strongly depends on the diameter of the cylindrical structure. We demonstrate that the angular dependence of radiation in external space for diameters just below guided-mode cut-off is highly directional whereas above cut-off emission is channeled into a newly formed guided mode.

Acknowledgments

The work has been supported by the Russian Science Foundation 21-12-00304.

References

[1] Lodahl P, Mahmoodian S, Stobbe S. Interfacing single photons and single quantum dots with photonic nanostructures. Rev Mod Phys 2015; 87(2): 347. DOI: 10.1103/RevModPhys.87.347.

[2] Senellart P, Solomon G, White, A. High-performance semiconductor quantum-dot single-photon sources. Nat Nanotechnol 2017; 12(11): 1026-1039. DOI: 10.1038/nnano.2017.218.

[3] Friedler I, Sauvan C, Hugonin JP, Lalanne P, Claudon J, Gérard JM. Solid-state single photon sources: the nanowire antenna. Opt Express 2009; 17(4): 2095-2110. DOI: 10.1364/OE.17.002095.

[4] Cihan AF, Curto AG, Raza S, [et al.]. Silicon Mie resonators for highly directional light emission from monolayer MoS2. Nat Photonics 2018; 12(5): 284-290. DOI: 10.1038/s41566-018-0155-y.

[5] Yan R, Gargas D, Yang P. Nanowire photonics. Nat Photonics 2009; 3(10): 569-576. DOI: 10.1038/nphoton.2009.184.

[6] Claudon J, Gregersen N, Lalanne P, Gérard J-M. Harnessing light with photonic nanowires: Fundamentals and applications to quantum optics. ChemPhysChem 2013; 14(11): 2393-2402. DOI: 10.1002/cphc.201300033.
[7] Claudon J, Bleuse J, Malik N, [et al.]. A highly efficient single-photon source based on a quantum dot in a photonic nanowire. Nat Photonics 2010; 4(3): 174-177. DOI: 10.1038/nphoton.2009.287x.
[8] Bleuse J, Claudon, J, Creasey M, Malik NS, Gérard J-M, Maksymov I, Hugonin J-P, Lalanne P. Inhibition, enhancement, and control of spontaneous emission in photonic nanowires. Phys Rev Lett 2011; 106: 103601. DOI: 10.1103/PhysRevLett.106.103601.
[9] Paniagua-Domínguez R, Grzela G, Rivas JG, Sánchez-Gil JA. Enhanced and directional emission of semiconductor nanowires tailored through leaky/guided modes. Nanoscale 2013; 5(21): 10582. DOI: 10.1039/c3nr03001f.
[10] Takahara J, Yamagishi S, Taki H, Morimoto A, Kobayashi T. Guiding of a one-dimensional optical beam with nanometer diameter. Opt Lett 1997; 22(7): 475-477. DOI: 10.1364/OL.22.000475.
[11] Leandro L, Gunnarsson CP, Reznik R, Jöns KD, Shtrom I, Khrebtov A, Kasama T, Zwiller V, Cirlin G, Akopian N. Nanowire quantum dots tuned to atomic resonances. Nano Lett 2018; 18(11): 7217-7221. DOI: 10.1021/acs.nanolett.8b03363.
[12] Reznik RR, Cirlin GE, Kotlyar KP, Ilkiv IV, Akopian N, Leandro L, Nikolaev VV, Belonovski AV, Kaliteevski MA. Purcell effect and beaming of emission in hybrid AlGaAs nanowires with GaAs quantum dots. Nanomaterials 2021; 11: 2894. DOI: 10.3390/nano11112894.
[13] Bulgarini G, Reimer ME, Bavinck MB, Jöns KD, Dalacu D, Poole PJ, Bakkers EPAM, Zwiller V. Nanowire waveguides launching single photons in a Gaussian mode for ideal fiber coupling. Nano Lett 2014; 14(7): 4102-4106. DOI: 10.1021/nl501648f.
[14] Bulgarini G, Reimer ME, Zehender T, Hocevar M, Bakkers EPAM, Kouwenhoven LP, Zwiller V. Spontaneous emission control of single quantum dots in bottom-up nanowire waveguides. Appl Phys Lett 2012; 100: 121106. DOI: 10.1063/1.3694935.
[15] Jeannin M, Cremel T, Häyrynen T, Gregersen N, Bellet-Amalric E, Nogues G, Kheng K. Enhanced photon extraction from a nanowire quantum dot using a bottom-up photonic shell. Phys Rev Appl 2017; 8: 054022. DOI: 10.1103/PhysRevApplied.8.054022.
[16] Haffouz S, Zeuner KD, Dalacu D, Poole PJ, Lapointe J, Poitras D, Mnaymneh K, Wu X, Couillard M, Korkusinski M, Schöll E, Jöns KD, Zwiller V, Williams RL. Bright single InAsP quantum dots at telecom wavelengths in position-controlled InP nanowires: The role of the photonic waveguide. Nano Lett 2018; 18(5): 3047-3052. DOI: 10.1021/acs.nanolett.8b00550.
[17] Jaffal A, Redjem W, Regreny P, Nguyen HS, Cueff S, Letartre X, Patriarche G, Rousseau E, Cassabois G, Gendry M, Chauvin N. InAs quantum dot in a needlelike tapered InP nanowire: a telecom band single photon source monolithically grown on silicon. Nanoscale 2019; 11: 21847-21855. DOI: 10.1039/C9NR06114B.
[18] Katsenelenbaum BZ. Symmetric and non-symmetric excitation of an infinite dielectric cylinder [In Russian]. Zhurnal Tekhnicheskoi Fiziki 1949; 19(10): 1168-1181.
[19] Yip GL. Launching efficiency of the HE11 surface wave mode on a dielectric rod. IEEE Trans Microw Theory Tech 1070; 18(12): 1033-1041. DOI: 10.1109/TMTT.1970.1127408.
[20] Chu DY, Ho S-T. Spontaneous emission from excitons in cylindrical dielectric waveguides and the spontaneous-emission factor of microcavity ring lasers. J Opt Soc Am B 1993; 10: 381-390. DOI: 10.1364/JOSAB.10.000381.
[21] Nha H, Jhe W. Cavity quantum electrodynamics for a cylinder: Inside a hollow dielectric and near a solid dielectric cylinder. Phys Rev A 1997; 56: 2213. DOI: 10.1103/PhysRevA.56.2213.
[22] Żakowicz W, Janowicz M. Spontaneous emission in the presence of a dielectric cylinder. Phys Rev A 2000; 62: 013820. DOI: 10.1103/PhysRevA.62.013820.
[23] Søndergaard T, Tromborg B. General theory for spontaneous emission in active dielectric microstructures: Example of a fiber amplifier. Phys Rev A 2001; 64: 033812. DOI: 10.1103/PhysRevA.64.033812.
[24] Klimov VV, Ducloy M. Spontaneous emission rate of an excited atom placed near a nanofiber. Phys Rev A 2004; 69: 013812. DOI: 10.1103/PhysRevA.69.013812.
[25] Kien FL, Liang JQ, Hakuta K, Balykin VI. Field intensity distributions and polarization orientations in a vacuum-clad subwavelength-diameter optical fiber. Opt Commun 2004; 242(4-6): 445-455. DOI: 10.1016/j.optcom.2004.08.044.
[26] Maslov, A. V. Bakunov, M. I. and Ning. C. Z. Distribution of optical emission between guided modes and free space in a semiconductor nanowire. J Appl Phys 2006; 99: 024314. DOI: 10.1063/1.2164538.
[27] Henderson MR, Afshar V S, Greentree AD, Monro TM. Dipole emitters in fiber: interface effects, collection efficiency and optimization. Opt Express 2011; 19: 16182-16194. DOI: 10.1364/OE.19.016182.
[28] Nikolaev VV, Ivanov KA, Morozov KM, Belonovski AV. Scattering matrix method for calculating spontaneous emission probability in cylindrically symmetrical structures. Semiconductors 2020; 54: 765-773. DOI: 10.1134/S1063782620070106.
[29] Abujetas DR, Paniagua-Domínguez R, Sánchez-Gil JA. Unraveling the Janus role of Mie resonances and leaky/guided modes in semiconductor nanowire absorption for enhanced light harvesting. ACS Photonics 2015; 2(7): 921-929. DOI: 10.1021/acsphotonics.5b00112.
[30] van Dam D, Abujetas DR, Paniagua-Domínguez R, Sánchez-Gil JA, Bakkers EPAM, Haverkort JEM, Rivas JG. Directional and polarized emission from nanowire arrays. Nano Lett 2015; 15(7): 4557-4563. DOI: 10.1021/acs.nanolett.5b01135.
[31] Ruda HE, Shik A. Polarization-sensitive optical phenomena in semiconducting and metallic nanowires. Phys Rev B 2005; 72: 115308. DOI: 10.1103/PhysRevB.72.115308.
[32] Arruda TJ, Bachelard R, Weiner J, Courteille PW. Tunable Fano resonances in the decay rates of a pointlike emitter near a graphene-coated nanowire. Phys Rev B 2018; 98: 245419. DOI: 10.1103/PhysRevB.98.245419.
[33] Barker AS, Ilegems M. Infrared lattice vibrations and free-electron dispersion in GaN. Phys Rev B 1973; 7: 743-750. DOI: 10.1103/PhysRevB.7.743.
[34] Deshpande S, Frost T, Yan L, Jahangir S, Hazari A, Liu X, Mirecki-Millunchick J, Mi Z, Bhattacharya P. Formation and nature of InGaN quantum dots in GaN nanowires, Nano Lett 2015; 15(3): 1647-1653. DOI: 10.1021/nl5041989.
[35] Vahala K. Optical microcavities. Nature 2003; 424: 839-846. DOI: 10.1038/nature01939.

Supplementary A: Cylindrical waves outside a cylinder

If the transverse wavenumber $k_{\rho 1}$ and the parameter x_1 are real (see Eq. (1)) the cylindrical waves in external medium are propagating and the components of TM polarized waves are proportional to the following dimensionless field profiles:

$$\begin{aligned}&\left(\tilde{\mathbf{E}}_{TM,m}^{Ext+/-}\right)_z=\frac{1}{2}\frac{1}{\sqrt{\varepsilon_1\mu_1}}\frac{x_1}{q}H_m^{(1/2)}\left(x_1\tilde{\rho}\right),\qquad \left(\tilde{\mathbf{E}}_{TMm}^{Ext+/-}\right)_\phi=-\frac{1}{2}\frac{m}{\sqrt{\varepsilon_1\mu_1}}\frac{\tilde{z}}{q}\frac{H_m^{(1/2)}\left(x_1\tilde{\rho}\right)}{x_1\tilde{\rho}},\\&\left(\tilde{\mathbf{E}}_{TM,m}^{Ext+/-}\right)_\rho=i\frac{1}{2}\frac{1}{\sqrt{\varepsilon_1\mu_1}}\frac{\tilde{z}}{q}H_m'^{(1/2)}\left(x_1\tilde{\rho}\right),\end{aligned}\tag{A1}$$

where $\tilde{\rho}=\rho/\rho_0$ is the distance from the symmetry axis reduced to the radius of the cylindrical structure. Hankel functions of the first (second) kind enter expressions designated by plus (minus) superscript and stand for divergent (convergent) waves.

TE polarized waves have two nonzero electric components:

$$\left(\tilde{\mathbf{E}}_{TE,m}^{Ext+/-}\right)_\phi=-i\frac{1}{2}H_m'^{(1/2)}\left(x_1\tilde{\rho}\right),\qquad \left(\tilde{\mathbf{E}}_{TE,m}^{Ext+/-}\right)_\rho=-\frac{1}{2}m\frac{H_m^{(1/2)}\left(x_1\tilde{\rho}\right)}{x_1\tilde{\rho}}.\tag{A2}$$

The asymptotic form of the cylindrical waves at large distances from the symmetry axis is:

$$\begin{aligned}&\mathbf{E}_{TM,m}^{Ext+/-}\left(\mathbf{r}\right)=\tilde{\mathbf{E}}_{TM,m}^{Ext+/-}\left(\rho\right)\times\exp\left(i\left[k_z z+m\phi\right]\right)\approx-\mathbf{e}_\theta\frac{e^{im\phi}\exp\left(\mp i\left(m\frac{\pi}{2}+\frac{\pi}{4}\right)\right)}{\sqrt{2\pi x_1\tilde{\rho}}}\exp\left(\pm i\left[k_{\rho 1}\rho+k_z z\right]\right),\\&\mathbf{E}_{TE,m}^{Ext+/-}\left(\mathbf{r}\right)=\tilde{\mathbf{E}}_{TE,m}^{Ext+/-}\left(\rho\right)\times\exp\left(i\left[k_z z+m\phi\right]\right)\approx\mathbf{e}_\phi\frac{e^{im\phi}\exp\left(\mp i\left(m\frac{\pi}{2}+\frac{\pi}{4}\right)\right)}{\sqrt{2\pi x_1\tilde{\rho}}}\exp\left(\pm i\left[k_{\rho 1}\rho+k_z z\right]\right).\end{aligned}\tag{A3}$$

where $\mathbf{e}_\theta$ is a unit vector corresponding to the spherical coordinate θ. Thus at large distances from the axis and in local regions of space cylindrical waves transform into orthogonal plain waves.

For imaginary $k_{\rho 1}$ and x_1 the TM-polarized field profile has a form:

$$\begin{aligned}&\left(\tilde{\mathbf{E}}_{TM,m}^{Ext+/-}\right)_z=\frac{1}{2}\frac{1}{\sqrt{\varepsilon_1\mu_1}}\frac{x_1}{q}Z_m^{(1/2)}\left(x_1\tilde{\rho}\right),\qquad \left(\tilde{\mathbf{E}}_{TM,m}^{Ext+/-}\right)_\phi=-\frac{1}{2}\frac{m}{\sqrt{\varepsilon_1\mu_1}}\frac{\tilde{z}}{q}\frac{Z_m^{(1/2)}\left(x_1\tilde{\rho}\right)}{x_1\tilde{\rho}},\\&\left(\tilde{\mathbf{E}}_{TM,m}^{Ext+/-}\right)_\rho=\frac{1}{2}\frac{1}{\sqrt{\varepsilon_1\mu_1}}\frac{\tilde{z}}{q}Z_m'^{(1/2)}\left(x_1\tilde{\rho}\right).\end{aligned}\tag{A4}$$

where expressions with plus superscripts contain functions $Z_m^{(1)}\left(x\right)=I_m\left(\left|x\right|\right)$ which exponentially increase with the distance from the symmetry axis and waves with minus superscript contain exponentially decreasing functions $Z_m^{(2)}\left(x\right)=K_m\left(\left|x\right|\right)$ (see Eq. (12)).

TE-polarized exponentially-changing electric fields are

$$\left(\tilde{\mathbf{E}}_{TE,m}^{Ext+/-}\right)_\phi=-\frac{1}{2}Z_m'^{(1/2)}\left(x_1\tilde{\rho}\right),\qquad \left(\tilde{\mathbf{E}}_{TE,m}^{Ext+/-}\right)_\rho=-\frac{1}{2}m\frac{Z_m^{(1/2)}\left(x_1\tilde{\rho}\right)}{x_1\tilde{\rho}}.\tag{A5}$$

At large distance from the axis $\tilde{\mathbf{E}}^{+/-}\propto\exp(\pm|x_1|\tilde{\rho})$ for both polarizations.

Supplementary B: Cylindrical fields inside a cylinder

If the value of parameter x_2 is real (i.e. the internal transverse wavenumber $k_{\rho 2}$ is real, see Eq. (1)) TM-polarized electric-field profile inside the cylinder can be written as:

$$\begin{aligned}&\left(\tilde{\mathbf{E}}_{TM,m}^{Int}\right)_z=\frac{1}{\sqrt{\varepsilon_2\mu_2}}\frac{x_2}{q}J_m\left(x_2\tilde{\rho}\right),\qquad \left(\tilde{\mathbf{E}}_{TM,m}^{Int}\right)_\phi=-\frac{m}{\sqrt{\varepsilon_2\mu_2}}\frac{\tilde{z}}{q}\frac{J_m\left(x_2\tilde{\rho}\right)}{x_2\tilde{\rho}},\\&\left(\tilde{\mathbf{E}}_{TM,m}^{Int}\right)_\rho=i\frac{1}{\sqrt{\varepsilon_2\mu_2}}\frac{\tilde{z}}{q}J_m'\left(x_2\tilde{\rho}\right),\end{aligned}\tag{B1}$$

where J_m is the Bessel function of the first order. The nonzero components of TE field are:

$$\left(\tilde{\mathbf{E}}^{Int}_{TE,m}\right)_{\phi} = -iJ'_m\left(x_2\tilde{\rho}\right), \qquad \left(\tilde{\mathbf{E}}^{Int}_{TE,m}\right)_{\rho} = -m\frac{J_m\left(x_2\tilde{\rho}\right)}{x_2\tilde{\rho}}. \tag{B2}$$

Let us consider electric field at the symmetry axis. Only TM polarized mode demonstrate nonzero axial electric field at the axis:

$$\tilde{\mathbf{E}}^{Int}_{TM,m=0}\left(\mathbf{r}=0\right) = \frac{1}{\sqrt{\varepsilon_2\mu_2}}\frac{x_2}{q}\mathbf{e}_z\ , \tag{B3}$$

The nonzero radial electric field at the axis is present only for TM/TE modes with $m=\pm1$:

$$\begin{aligned}
&\tilde{\mathbf{E}}^{Int}_{TM,m=\pm1}\left(\mathbf{r}=0\right) = \tilde{\mathbf{E}}^{Int}_{TM,m=\pm1}\left(\rho=0\right)\exp\left(\pm i\phi\right) = \pm i\frac{1}{\sqrt{2}}\frac{1}{\sqrt{\varepsilon_2\mu_2}}\frac{\tilde{z}}{q}\times\frac{1}{\sqrt{2}}\left(\mathbf{e}_x \pm i\mathbf{e}_y\right),\\
&\tilde{\mathbf{E}}^{Int}_{TE,m=\pm1}\left(\mathbf{r}=0\right) = \tilde{\mathbf{E}}^{Int}_{TE,m=\pm1}\left(\rho=0\right)\exp\left(\pm i\phi\right) = -\frac{1}{\sqrt{2}}\times\frac{1}{\sqrt{2}}\left(\mathbf{e}_x \pm i\mathbf{e}_y\right).
\end{aligned} \tag{B4}$$

The modes with $|m|>1$ have zero electric field at the symmetry axis.

The expression of TM-polarized field for imaginary x_2 is

$$\begin{aligned}
&\left(\tilde{\mathbf{E}}^{Int}_{TM,m}\right)_z = \frac{1}{2}\frac{1}{\sqrt{\varepsilon_2\mu_2}}\frac{x_2}{q}I_m\left(|x_2|\tilde{\rho}\right), \qquad \left(\tilde{\mathbf{E}}^{Int}_{TM,m}\right)_{\phi} = -\frac{1}{2}\frac{m}{\sqrt{\varepsilon_2\mu_2}}\frac{\tilde{z}}{q}\frac{1}{x_2\tilde{\rho}}I_m\left(|x_2|\tilde{\rho}\right),\\
&\left(\tilde{\mathbf{E}}^{Int}_{TM,m}\right)_{\rho} = i\frac{1}{2}\frac{1}{\sqrt{\varepsilon_2\mu_2}}\frac{\tilde{z}}{q}I'_m\left(|x_2|\tilde{\rho}\right),
\end{aligned} \tag{B5}$$

where only the modified Bessel function I_m is preserved due to its finiteness at zero argument.

The TE-polarized field inside the cylinder for imaginary x_2 can be written as:

$$\left(\tilde{\mathbf{E}}^{Int}_{TE,m}\right)_{\phi} = -iI'_m\left(|x_2|\tilde{\rho}\right), \qquad \left(\tilde{\mathbf{E}}^{Int}_{TE,m}\right)_{\rho} = -\frac{m}{x_2\tilde{\rho}}I_m\left(|x_2|\tilde{\rho}\right). \tag{B6}$$

The electric fields at the axis for modes with imaginary x_2 are similar to the aforementioned case of real x_2.

Authors' information

Valentin Nikolaev, (b. 1978) graduated from Peter the Great St. Petersburg Polytechnic University in 2001. He received his PhD in Physics degree from the University of Exeter, UK, in 2002 and his Candidate in Physics & Maths degree from Ioffe Institute, St. Petersburg, Russia in 2005. He worked as a researcher in University of York, Ioffe Institute and Submicron Heterostructures for Microelectronics Research and Engineering Center of the Russian Academy of Science. His current research interests include nanophotonics and optics of semiconductor nanostructures.
E-mail: valia.nikolaev@gmail.com .

Elizaveta Ilinichna Girshova (b. 1991) graduated from Saint-Petersburg State University in 2016. Currently she works as an engineer in Research Center for Advanced Functional Materials and Laser Communication Systems. Research interests are nanophotonics, optoacoustics, light-matter interaction. E-mail: ilinishna@gmail.com .

Mikhail Alekseevich Kaliteevski, (b. 1969), Dr, chief reseacher at ITMO University. Research interests: light-matter interaction, plasmonics, mesoresonators, nanophotonics, numerical simulation. E-mail: m.kaliteevski@gmail.com .

Received April 6, 2022. The final version – June 4, 2022.